

# A massive warm baryonic halo in the Coma cluster

Massimiliano Bonamente<sup>1,2</sup>, Marshall K. Joy<sup>2</sup> and Richard Lieu<sup>1</sup>

<sup>1</sup>*Department of Physics, University of Alabama, Huntsville, AL*

<sup>2</sup>*National Space Science and Technology Center, NASA/MSFC, Huntsville, AL*

## ABSTRACT

Several deep PSPC observations of the Coma cluster reveal a very large-scale halo of soft X-ray emission, substantially in excess of the well known radiation from the hot intra-cluster medium. The excess emission, previously reported in the central region of the cluster using lower-sensitivity EUVE and ROSAT data, is now evident out to a radius of 2.6 Mpc, demonstrating that the soft excess radiation from clusters is a phenomenon of cosmological significance. The X-ray spectrum at these large radii cannot be modeled non-thermally, but is consistent with the original scenario of thermal emission from warm gas at  $\sim 10^6$  K. The mass of the warm gas is on par with that of the hot X-ray emitting plasma, and significantly more massive if the warm gas resides in low-density filamentary structures. Thus the data lend vital support to current theories of cosmic evolution, which predict that at low redshift  $\sim 30$ -40 % of the baryons reside in warm filaments converging at clusters of galaxies.

*Subject headings:* X-rays: galaxies: clusters, X-rays: individual (Coma cluster), Cosmology: large-scale structure of universe

## 1. Introduction

Clusters of galaxies are strong emitters of X-rays, which originate from a hot and diffuse intra-cluster medium (ICM). At the typical temperatures of a few  $\times 10^7$  K, the bulk of the hot ICM emission is detected at energies  $\geq 1$  keV, intervening Galactic absorption being responsible for a substantial reduction of flux below  $\sim 1$  keV. However, hot gas is not the only high energy component seen in clusters, and the extreme-ultraviolet (EUV) and soft X-ray band below  $\sim 1$  keV offer a unique window to investigate the presence of other phases in the ICM.

In 1996, Lieu et al. (1996) reported the discovery of excess EUV and soft X-ray emission above the contribution from the hot ICM in the Coma cluster; their conclusions were based

upon *Extreme UltraViolet Explorer (EUVE)* Deep Survey data (65-200 eV) and *ROSAT* PSPC data (0.15-0.3 keV). Subsequently, Bowyer, Berghoefer and Korpela (1999) reanalyzed the EUVE data and confirmed the existence of strong excess emission in the central 15' of Coma. Arabadjis and Bregman (1999) reanalyzed the PSPC data, and reported that the fitted HI column density in the center of the cluster was significantly smaller than the measured Galactic value, consistent with the earlier reports of soft X-ray excess emission. Recently, the spatial distribution of the soft X-ray emission in the center of the Coma cluster was investigated by Bonamente et al. (2002) and Nevalainen et al. (2002). In this paper we present the analysis of a mosaic of *ROSAT* PSPC observations around the Coma cluster, revealing a very diffuse soft X-ray halo extending to considerably larger distances than reported in the previous studies.

The nature of the excess emission has been under active scrutiny. The emission could originate from Inverse-Compton scattering of cosmic microwave background (CMB) photons against a population of relativistic electrons in the intra-cluster medium (ICM), as advocated by Hwang (1997), Sarazin and Lieu (1998), Ensslin and Biermann (1998) and Lieu et al. (1999). Alternatively, warm gas at  $T \sim 10^6$  K could be responsible for the soft emission (Lieu et al. 1996, Nevalainen et al. 2002). Warm gas may reside inside the cluster, or in very diffuse filamentary structures outside the cluster projecting onto it, as seen in large scale hydrodynamic simulations (e.g., Cen and Ostriker 1999, Davé et al. 2001, Cen et al 2001). The warm gas scenario appears to be favored by the current X-ray spectral analyses (e.g., Bonamente et al. 2001a, Buote 2001), although a search for the UV OVI emission lines (1032-1039 Å in rest frame) has not yielded positive results (Dixon, Hurwitz and Ferguson 1996; Dixon et al. 2001). The non-detection of emission lines can be reconciled with the soft excess detection if the gas has very low metal abundances, or alternatively if the gas exists in a temperature range where OVI is not the predominant oxygen ion. The spectral analysis of PSPC data reported in this paper indicates that the emission is very likely thermal in nature.

The PSPC observations are described in section 2, and the distribution of the Galactic HI over the field of view is presented in section 3. Analysis of the PSPC spectra is given in section 4, followed by the interpretation in section 5 and conclusions in section 6.

The redshift to the Coma cluster is  $z=0.023$  (Struble and Rood 1999). Throughout this paper we assume a Hubble constant of  $H_0 = 72 \text{ km s}^{-1} \text{ Mpc}^{-1}$  (Freedman et al. 2001), and all quoted uncertainties are at the 68% confidence level.

## 2. The ROSAT PSPC data

The *ROSAT* PSPC instrument has unique capabilities for the study of the low energy excess emission in clusters of galaxies. Along with an effective area of  $\sim 200 \text{ cm}^{-2}$  at 0.25 keV, the spectral response between 0.2 and 2 keV is well calibrated (Snowden et al. 1994). Moreover, the large field of view ( $\sim 1$  degree radius), low detector background and the availability of a large number of deep cluster observations and of the *ROSAT* All-Sky Survey data (RASS), render the PSPC a unique instrument to detect and investigate the large-scale diffuse emission from galaxy clusters.

Coma is the nearest rich galaxy cluster, and the X-ray emission from its hot ICM reaches an angular radius of at least 1 degree (e.g., White et al. 1993, Briel et al. 2001). If the soft X-ray background level is estimated from the edge of the PSPC field of view as is customarily done for more distant clusters, the background can be significantly overestimated due to the extended cluster emission (Bonamente et al. 2002). Here we show how several off-center PSPC observations provide a reliable measurement of the background and reveal a very extended halo of soft X-ray excess radiation, covering a region several megaparsecs in extent in the Coma cluster.

The RASS maps of the diffuse X-ray background (Snowden et al. 1997) are suitable to measure the extent of the soft X-ray emission (R2 band,  $\sim 0.15\text{-}0.3$  keV) around the Coma cluster and to compare it with that of the higher-energy X-ray emission (R7 band,  $\sim 1\text{-}2$  keV). In Fig. 1 we show a radial profile of the surface brightness of PSPC bands R2 and R7 centered on Coma: the higher-energy emission has reached a constant background value at a radius of  $\sim 1.5$  degrees, while the soft X-ray emission persists out to a radius of  $\sim 3$  degrees. Thus, the RASS data indicate that the soft emission is more extended than the 1-2 keV emission, which originates primarily from the hot phase of the ICM.

The all-sky survey data is based on very short exposures ( $\sim 700$  sec); therefore, for detailed studies of the soft X-ray emission in the Coma cluster, we use the four PSPC observations shown in Fig. 2. Four additional deep PSPC observations (also shown in Fig. 2) are used to determine the local background <sup>1</sup>. We show in section 3 below that the distribution of  $N_H$  is essentially constant within 5 degrees of the cluster center. Therefore, the off-source PSPC fields located 2.5-4 degrees away from the cluster center provide an accurate measurement of the soft X-ray background, and are also far enough away from the cluster center to avoid being contaminated by cluster X-ray emission (Fig. 1).

---

<sup>1</sup>The ROSAT archival ID of the Coma pointings are RP8000005N00,RP8000006N00,RP8000009N00 and RP8000013N00, the ID of the background fields are RP9002121A01,RP201514N00, RP201471N00, and RP141917N00.

### 3. Galactic HI absorption in the direction of the Coma cluster

Knowledge of the Galactic absorption is essential to determine the intrinsic X-ray emission from extragalactic objects, particularly at energies  $\leq 1$  keV. Throughout this paper, we use the absorption cross sections of Morrison and McCammon (1983) in our models. These cross sections are in good agreement with the recent compilation of Yan, Sadeghpour and Dalgarno (1998), as discussed by Arabadjis and Bregman (1999). At the resolution of the PSPC, the He cross section in the most recent compilation by Wilms, Allen and McCray (2000) is also indistinguishable from the values of Morrison and McCammon (1983), as discussed by Bonamente et al. (2002).

We use two methods to determine the distribution of neutral hydrogen in the Coma cluster. First, we use the radio measurements of Dickey and Lockman (1990) and of Hartmann and Burton (1997), which are plotted in Fig. 3. The radio measurements are in excellent agreement, and show the measured HI column density varying smoothly from  $9 \times 10^{19} \text{ cm}^{-2}$  to  $11 \times 10^{19} \text{ cm}^{-2}$  within a radius of 5 degrees from the center of the Coma cluster. Second, we employ the far-infrared IRAS data, and use the correlation between 100  $\mu\text{m}$  IRAS flux and HI column density (Boulanger and Perault 1988). The slope of the correlation is  $1.2 \times 10^{20} \text{ cm}^{-2} / (\text{MJy sr}^{-1})$ , and the offset is determined by fixing the central  $N_H$  value to  $9 \times 10^{19} \text{ cm}^{-2}$ , which is well established from independent radio measurements of the center of the Coma cluster (Dickey and Lockman 1990, Lieu et al. 1996, Hartmann and Burton 1997). Fig. 3 shows that the radial variation of  $N_H$  inferred from the IRAS data is in extremely good agreement with the radio measurements. The data indicate that

- (a) the HI column density within the central 1.5 degree of the cluster is constant ( $9 \pm 1 \times 10^{19} \text{ cm}^{-2}$ ), and
- (b) in the region where the off-source background fields are located (2.5-4 degrees from the cluster center), the HI column density is between  $9 \times 10^{19} \text{ cm}^{-2}$  and  $11 \times 10^{19} \text{ cm}^{-2}$ . An  $N_H$  variation of this magnitude has a negligible effect on the soft X-ray flux in the PSPC R2 band (cf. Fig. 5 in Snowden et al. 1998).

With the present IR and radio data we cannot address the possibility of variations in the HI distribution on scales smaller than  $\sim 10$  arcmin. On occasions for which a comparison with stellar Ly $\alpha$  and QSO X-ray spectra could be made, the  $N_H$  was found consistent with the wide-beam measurements to within  $\sim 1 \times 10^{19} \text{ cm}^{-2}$  (Laor et al. 1994; Elvis, Lockman and Wilkes 1989; Dickey and Lockman 1990).

## 4. Spectral analysis

The 4 PSPC Coma observations were divided into concentric annuli centered at R.A.=12h59'48", Dec.=25°57'0" (J2000), and the spectra were coadded to reduce the statistical errors. The pointed PSPC data were reduced according to the prescriptions of Snowden et al. (1994). The datasets were corrected for detector gain fluctuations, and only events with Average Master Veto rate  $\leq 170$  c/s were considered, in order to discard periods of high particle background. The PSPC rejection efficiency for particle background is 99.9 % in the 0.2-2 keV energy range (Plucinsky et al. 1993), and the background is therefore solely represented by the photonic component. For each of the 4 off-source fields in Fig. 1, a spectrum was extracted after removal of point sources. The spectra were statistically consistent with one another within at most  $\sim 10$  % point-to-point fluctuations. The off-source spectra were therefore coadded, and a 10% systematic uncertainty in the background was included in the error analysis. Further details of the PSPC data analysis can be found in Bonamente et al. (2002).

### 4.1. Single temperature fits

Initially, we fit the spectrum of each annulus in XSPEC, using a single-temperature MEKAL plasma model (Mewe, Gronenschild and van den Oord 1985; Mewe, Lemen and van den Oord 1986; Kaastra 1992) and the WABS Galactic absorption model (Morrison and McCammon 1983). The results of the single temperature fit are given in Table 1, and are shown for one of the annuli in Fig. 4. If the neutral hydrogen column density is fixed at the Galactic value ( $9 \times 10^{19} \text{ cm}^{-2}$ , see section 3), the fits are statistically unacceptable (reduced  $\chi^2$  ranging from 3.1 to 9.7). Allowing the neutral hydrogen column density to vary results in an unrealistically low  $N_H$  for all of the annuli, and also produces statistically unacceptable fits (reduced  $\chi^2$  ranging from 2.5 to 4.2). We conclude that a single temperature plasma model does not adequately describe the spectral data, particularly at energies below 1 keV (Fig. 4). Therefore, in the analysis that follows, we fit only the high energy portion of the spectrum (1-2 keV) with a single temperature plasma model, and introduce an additional model component to account for the low energy emission.

### 4.2. Modelling the hot ICM

To fit the high energy portion of the spectrum, we apply a MEKAL model to the data between 1 and 2 keV, and a photoelectric absorption model with  $N_H = 9 \times 10^{19} \text{ cm}^{-2}$ . The

metal abundance is fixed at 0.25 solar for the central 20 arcmin region (Arnaud et al. 2001), and at 0.2 solar in the outer regions. The spectra are also subdivided into quadrants, in order to obtain a more accurate temperature for each region of the cluster. The results of the ‘hot ICM’ fit are given in Table 2, and are consistent with the results previously derived from the PSPC data by Briel and Henry (1997), and with recent XMM measurements (Arnaud et al. 2001). In addition, the temperature found at large radii is in agreement with the composite cluster temperature profile of De Grandi and Molendi (2002).

### 4.3. Soft excess emission

The measured fluxes in the soft X-ray band can now be compared with the hot ICM model predictions in the 0.2-1 keV band. The results are shown in Table 2 and Fig. 5. The error bars reflect the uncertainty in the hot ICM temperature (Table 2) and the uncertainty in the Galactic HI column density ( $N_H = 9 \pm 1 \times 10^{19} \text{ cm}^{-2}$ ). The soft excess component is detected with high statistical significance throughout the 90’ radius of the pointed PSPC data, which corresponds to a radial distance of 2.6 Mpc. The soft excess emission (Fig. 5, left panel) is much more extended than that of the hot ICM (Fig. 5, right panel), in agreement with the conclusions drawn from the all-sky survey data (Fig. 1).

### 4.4. Low energy non-thermal component

Having established the hot ICM temperature for each quadrant (Table 2), we now consider additional components in the spectral analysis. First, we add a power law non-thermal component, which predominantly contributes to the low energy region of the spectrum (Sarazin and Lieu 1998). The neutral hydrogen column density was fixed at the Galactic value ( $N_H = 9 \times 10^{19} \text{ cm}^{-2}$ ). The results of fitting the hot ICM plus power law models to the annular regions are shown in Table 3. The reduced  $\chi^2$  values are poor: the average  $\chi_{red}^2$  is 1.48, and the worst case value is 1.89; we conclude that the combination of a low energy power law component and the hot ICM thermal model does not adequately describe the PSPC spectral data.

### 4.5. Low energy thermal component

Finally, we consider a model consisting of a ‘hot ICM’ thermal component (section 4.2) and an additional low-temperature thermal component. As before, the neutral hydrogen

column density was fixed at the Galactic value (see section 3). The results of fitting the hot ICM plus warm thermal models are shown in Table 3. The reduced  $\chi^2$  values are significantly improved relative to the previous case: the average reduced  $\chi^2$  is 1.24 and the worst case value is 1.45. In every region the fit obtained with a warm thermal component was superior to the fit using a non-thermal component, as indicated by inspection of the  $\chi_{red}^2$  values and by an F-test (Bevington 1969) on the two  $\chi^2$  distributions (Table 3).

## 5. Interpretation

The spectral analysis of section 4 indicates that the excess emission can be explained as thermal radiation from diffuse warm gas. The non-thermal model appears viable only in a few quadrants, and will not be further considered in this paper.

### 5.1. A warm phase of the ICM

If the soft excess emission originates from a warm phase of the intra-cluster medium, the ratio of the emission integral of the hot ICM (Table 2) and the emission integral of the warm gas (Table 3) can be used to measure the relative mass of the two phases. The emission integral is defined as

$$I = \int n^2 dV, \quad (1)$$

where  $n$  is the gas density and  $dV$  is the volume of emitting region (Sarazin 1988). The emission integral is readily measured by fitting the X-ray spectrum.<sup>2</sup>

The emission integral of each quadrant determines the average density of the gas in that region, once the volume of the emitting region is specified (Eq. 1). Assuming that each quadrant corresponds to a sector of a spherical shell, the density in each sector can be calculated. The density of the warm gas ranges from  $\sim 9 \times 10^{-4} \text{ cm}^{-3}$  to  $\sim 8 \times 10^{-5} \text{ cm}^{-3}$ , and the density of the hot gas varies from  $1.5 \times 10^{-3} \text{ cm}^{-3}$  to  $6 \times 10^{-5} \text{ cm}^{-3}$ .

We assume that both the warm gas and the hot gas are distributed in spherical shells of constant density. Since the emission integral is proportional to  $n^2 dV$  and the mass is proportional to  $n dV$ , the ratio of the warm-to-hot gas mass is

$$\frac{M_{warm}}{M_{hot}} = \frac{\int n_{warm} dV}{\int n_{hot} dV} = \frac{\int dI_{warm}/n_{warm}}{\int dI_{hot}/n_{hot}} \quad (2)$$

---

<sup>2</sup>See description of XSPEC MEKAL model at <http://heasarc.gsfc.nasa.gov/docs/xanadu/xspec/manual/manual.html>.

We evaluate Eq. 2 by summing the values of  $I_{hot}/n_{hot}$  and  $I_{warm}/n_{warm}$  for all regions (Tables 2 and 3), and conclude that  $M_{warm}/M_{hot}=0.75$  within a radius of 2.6 Mpc.

## 5.2. Warm filaments around the Coma cluster

It is also possible that the warm gas is distributed in extended low-density filaments rather than being concentrated near the cluster center like the hot ICM. Recent large-scale hydrodynamic simulations (e.g., Cen et al. 2001, Davé et al. 2001, Cen and Ostriker 1999) indicate that this is the case, and that 30-40 % of the present epoch’s baryons reside in these filamentary structures. Typical filaments feature a temperature of  $T \sim 10^5 - 10^7$  K, consistent with our results in Table 3, and density of  $\sim 10^{-5} - 10^{-4} \text{ cm}^{-3}$  (overdensity of  $\delta \sim 30 - 300$ , Cen et al. 2001).

The ratio of mass in warm filaments to mass in the hot ICM is

$$\frac{M_{fil}}{M_{hot}} = \frac{\int n_{fil} dV_{fil}}{\int n_{hot} dV} = \frac{\int dI_{warm}/n_{fil}}{\int dI_{hot}/n_{hot}}. \quad (3)$$

Assuming a filament density of  $n_{fil} = 10^{-4} \text{ cm}^{-3}$ , Eq. (3) yields the conclusion that  $M_{fil}/M_{hot} = 3$  within a radius of 2.6 Mpc; the ratio will be even larger if the filaments are less dense. The warm gas is therefore more massive than the hot ICM if it is distributed in low-density filaments. More detailed mass estimates require precise knowledge of the filaments spatial distribution.

## 6. Conclusions

The analysis of deep PSPC data of the Coma cluster reveals a large-scale halo of soft excess radiation, considerably more extended than previously thought. The PSPC data indicate that the excess emission is due to warm gas at  $T \sim 10^6$  K, which may exist either as a second phase of the intra-cluster medium, or in diffuse filaments outside the cluster. Evidence in favor of the latter scenario is provided by the fact that the spatial extent of the soft excess emission is significantly greater than that of the hot ICM.

The total mass of the Coma cluster within 14 Mpc is  $1.6 \pm 0.4 \times 10^{15} M_{\odot}$  (Geller, Diaferio and Kurtz). The mass of the hot ICM is  $\sim 4.3 \times 10^{14} M_{\odot}$  within 2.6 Mpc (Mohr, Mathiesen and Evrard 1999). The present detection of soft excess emission out to a distance of 2.6 Mpc from the cluster’s center implies that the warm gas has a mass of at least  $3 \times 10^{14} M_{\odot}$ , or considerably larger if the gas is in very low density filaments. The PSPC data presented



in this paper therefore lends observational support to the current theories of large-scale formation and evolution (e.g, Cen and Ostriker 1999), which predict that a large fraction of the current epoch’s baryons are in a diffuse warm phase of the intergalactic medium.

## REFERENCES

- Arabadjis, J.S. and Bregman, J.N. 1999, ApJ, 514,607
- Arnaud, M. et al. 2001, A&A, 365, L67
- Bevington, P.R. 1969, Data reduction and error analysis for the physical sciences (McGraw-Hill)
- Blandford, R.D. and Ostriker, J.P. 1978, A&A, 221, L29
- Bonamente, M., Lieu, R., Joy, M.K. and Nevalainen, J.H. 2002, ApJ, 576, 688
- Bonamente, M., Lieu, R. and Mittaz, J.P.D. 2001a, ApJ, 547,7
- Boulinger, F. and Perault, M. 1988, ApJ, 330, 964
- Bowyer, S., Berghoefer, T.W. and Korpela, E.J. 1999, ApJ, 526, 592
- Briel, U.G. et al. 2001, A&A, 365, L60
- Briel, U.G. and Henry, J.P. 1997, *Proc. of the conference ‘A New Vision of an old cluster: Untangling Coma Berenices’* Eds. A. Mazure, F. Casoli, F. Durret and D. Gerbal, pp. 170
- Buote, D.A., 2001, ApJ, 548, 652
- Cen, R. and Ostriker, J.P. 1999, ApJ, 514, L1
- Cen, R., Tripp, T.M., Ostriker, J.P. and Jenkins, E.B. 2001, ApJ, 559,L5
- Davé, R., Cen, R., Ostriker, J.P., Bryan, G.L., Hernquist, L., Katz, N., Weinberg, D.H., Norman, M.L. and O’Shea, B. 2001, ApJ, 552, 473
- De Grandi, S. and Molendi, S. 2002, ApJ, 567, 163
- Dickey, J.M. and Lockman, F.J. 1990, ARA&A, 28, 215
- Dixon, W.V., Sallmen, S., Hurwitz, M., & Lieu, R., 2001, ApJ, 550,L25

- Dixon, W.V., Hurwitz, M., & Ferguson, H.C., 1996, *ApJ*, 469, L77
- Elvis, M., Wilkes, B.J. and Lockman, F.J. 1989, *AJ*, 97, 777
- Freedman, W.L. et al. 2001, *ApJ*, 553, 47
- Geller, M.J., Diaferio, A. and Kurtz, M.J. 1999, *ApJ*, 517, L26
- Hartmann, D. and Burton, W.B. 1997, *Atlas of Galactic Neutral Hydrogen* (Cambridge: Cambridge Univ. Press)
- Hwang, C.-Y. 1997, *Science*, 278, 1917
- Kaastra, J.S. 1992 in ‘An X-Ray Spectral Code for Optically Thin Plasmas’ (Internal SRON-Leiden Report, updated version 2.0)
- Laor, A., Fiore, F., Elvis, M., Wilkes, B.J. and McDowell, J.C. 1994, *ApJ*, 435, 611
- Lieu, R., Ip, W.-I., Axford, W.I. and Bonamente, M. 1999b, *ApJ*, 510,L25
- Lieu, R., Mittaz, J.P.D., Bowyer, S., Breen, J.O., Lockman, F.J., Murphy, E.M. & Hwang, C. -Y. 1996b, *Science*, 274,1335
- Mewe, R., Gronenschild, E.H.B.M., and van den Oord, G.H.J., 1985 *A&A*62 S197
- Mewe, R., Lemen, J.R., and van den Oord, G.H.J. 1986, *A&A*65 511
- Mohr, J.J., Mathiesen, B and Evrard, A. E. 1999, *ApJ*, 517, 627
- Morrison, R. and McCammon, D. 1983, *ApJ*270 119
- Nevalainen, J.H., Lieu, R., Bonamente, M. and Oosterbroeck, T. 2002, *ApJ*, in press
- Plucinsky, P.P, Snowden, S.L., Briel, U.G., Hasinger, G. and Pfefferman, E. 1993, *ApJ*418 519 *A&A*, 134, S287
- Sarazin, C.L. 1988, *X-ray emission from clusters of galaxies*, Cambridge Astrophysics Series (Cambridge: Cambridge University Press)
- Sarazin, C.L. and Lieu, R. 1998, *ApJ*, 494, L177
- Snowden, S.L. et al. 1997, *ApJ*, 485, 125
- Snowden, S.L., Egger, R., Finkbeiner, D.P., Freyberg, M.J. and Plucinsky, P.P. 1998, *ApJ*, 493, 715

Snowden, S.L., McCammon, D., Burrows, D.N. and Mendenhall, J.A. 1994, ApJ424 714

Struble, M.F. and Rood, H.J. 1999, ApJS, 125, 35

Yan, M., Sadeghpour, H.R. and Dalgarno, A. 1998, ApJ496 1044

White, S.D.M., Briel, U.G. and Henry, J.P. 1993, MNRAS, 261, L8

Wilms, J., Allen, A. and McCray R. 2000 ApJ542 914

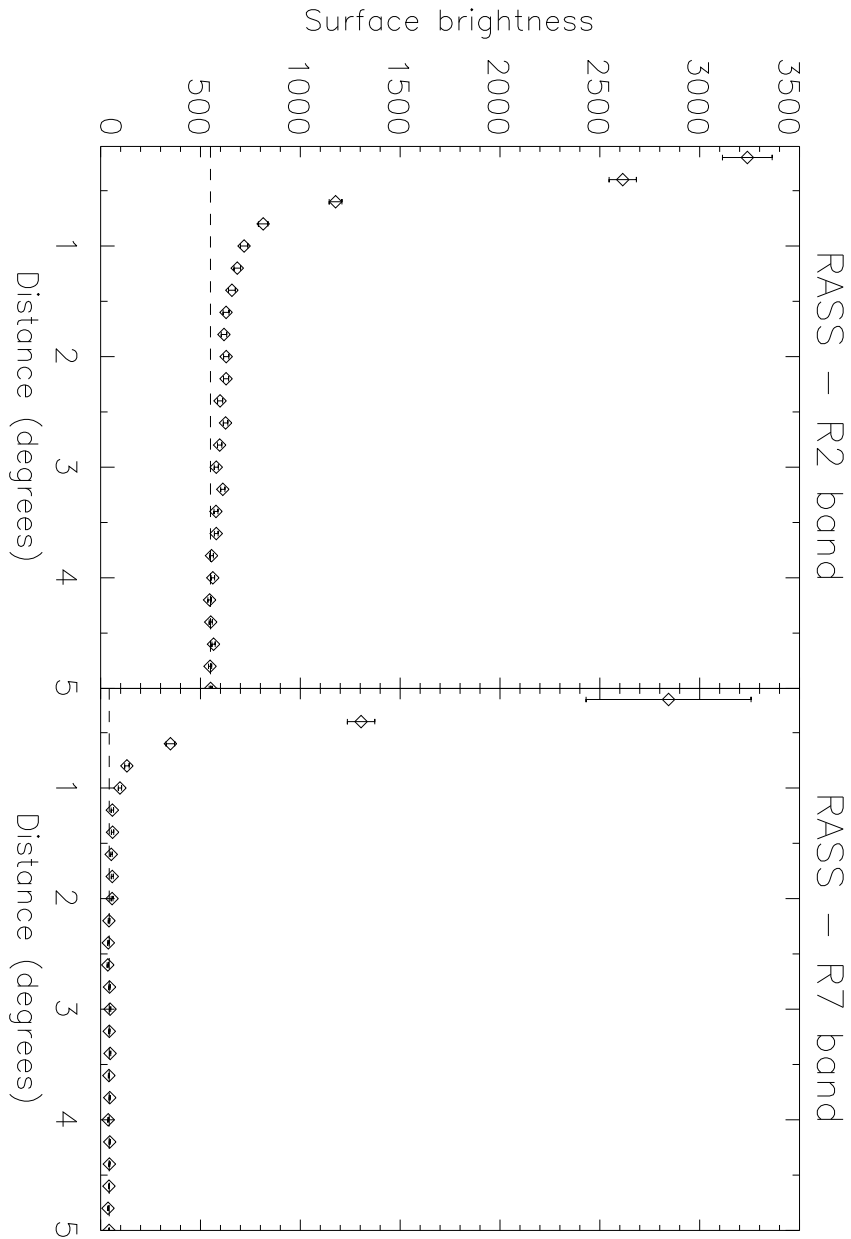


Fig. 1.— Radial profiles of soft X-ray emission (R2 band, 0.15-0.3 keV) and higher energy X-ray emission (R7 band, 1-2 keV) in the Coma cluster. Surface brightness units are  $10^{-6}$  counts  $\text{s}^{-1}$   $\text{arcmin}^{-2}$   $\text{pixel}^{-1}$  (Snowden et al. 1998)

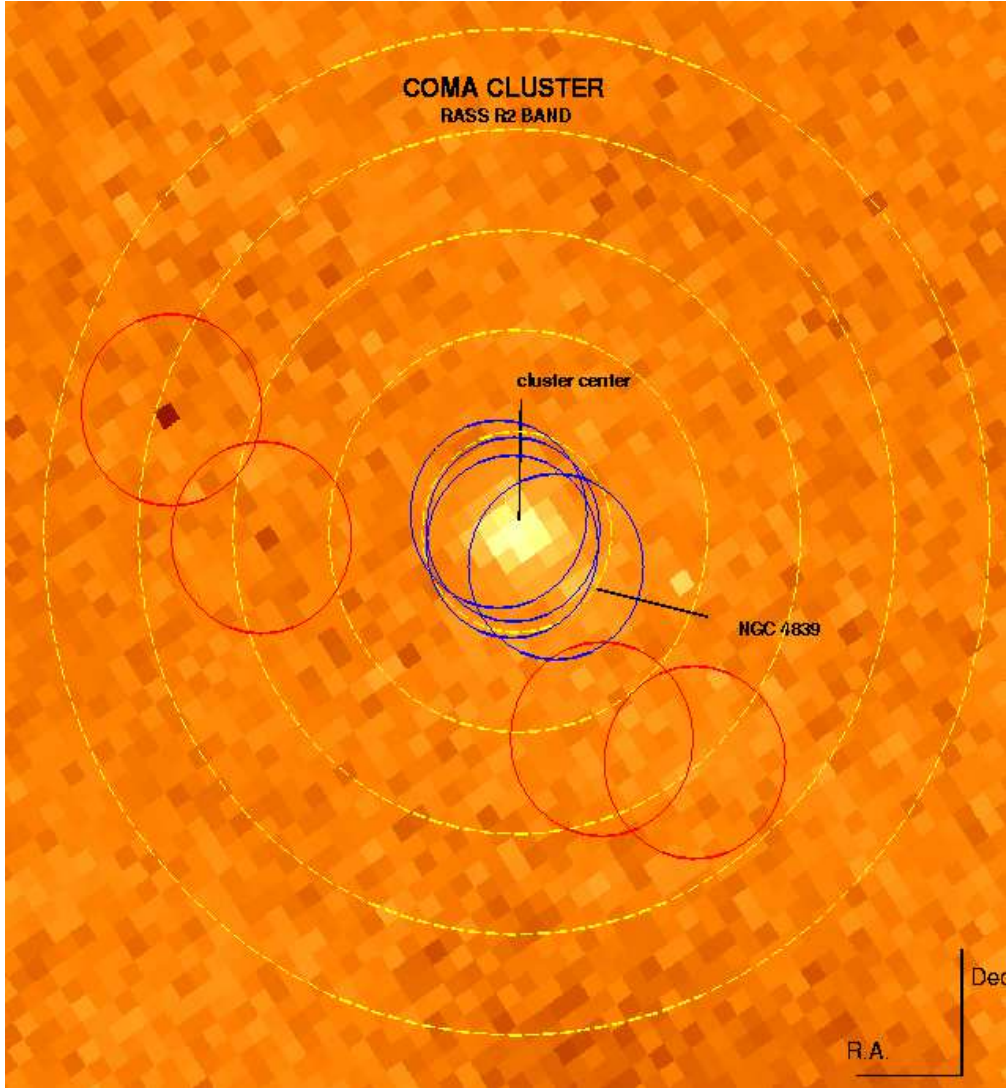


Fig. 2.— Location of *ROSAT* PSPC observations, overlaid on a RASS R2 band (0.15-0.3 keV) image of the diffuse emission of the Coma region. Dashed circles indicate distance from the cluster’s center in intervals of 1 degree, blue circles represent the position of the pointed PSPC observations of Coma cluster, red circles are background observations.

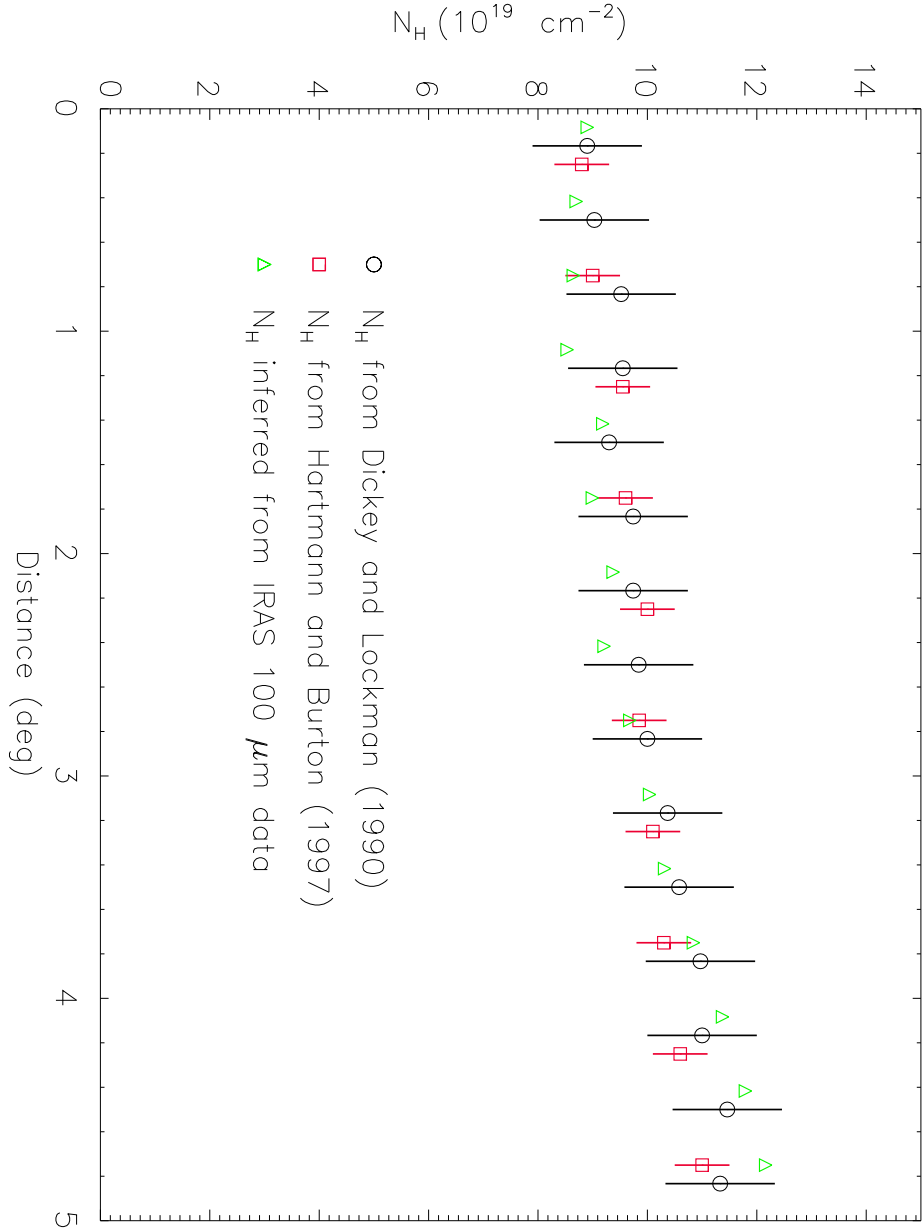


Fig. 3.— The Galactic  $N_H$  distribution around the Coma cluster from the Dickey and Lockman (1990) radio survey data, the Hartmann and Burton (1997) radio data, and as inferred from IRAS 100  $\mu\text{m}$  data. Errors in the IRAS measurements are estimated to be less than  $2 \times 10^{19} \text{ cm}^{-2}$  (Boulanger and Perault 1988).

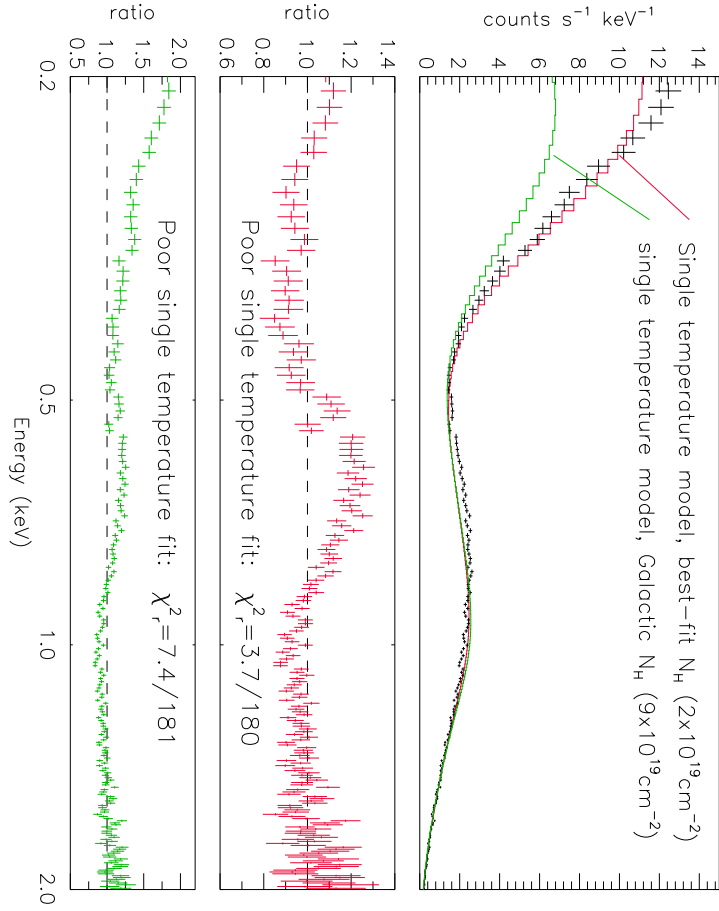


Fig. 4.— *ROSAT* PSPC spectrum of the 20-40' region around the center of the Coma cluster, fitted to a single temperature model with variable  $N_H$  (red), and with Galactic  $N_H$  (green).

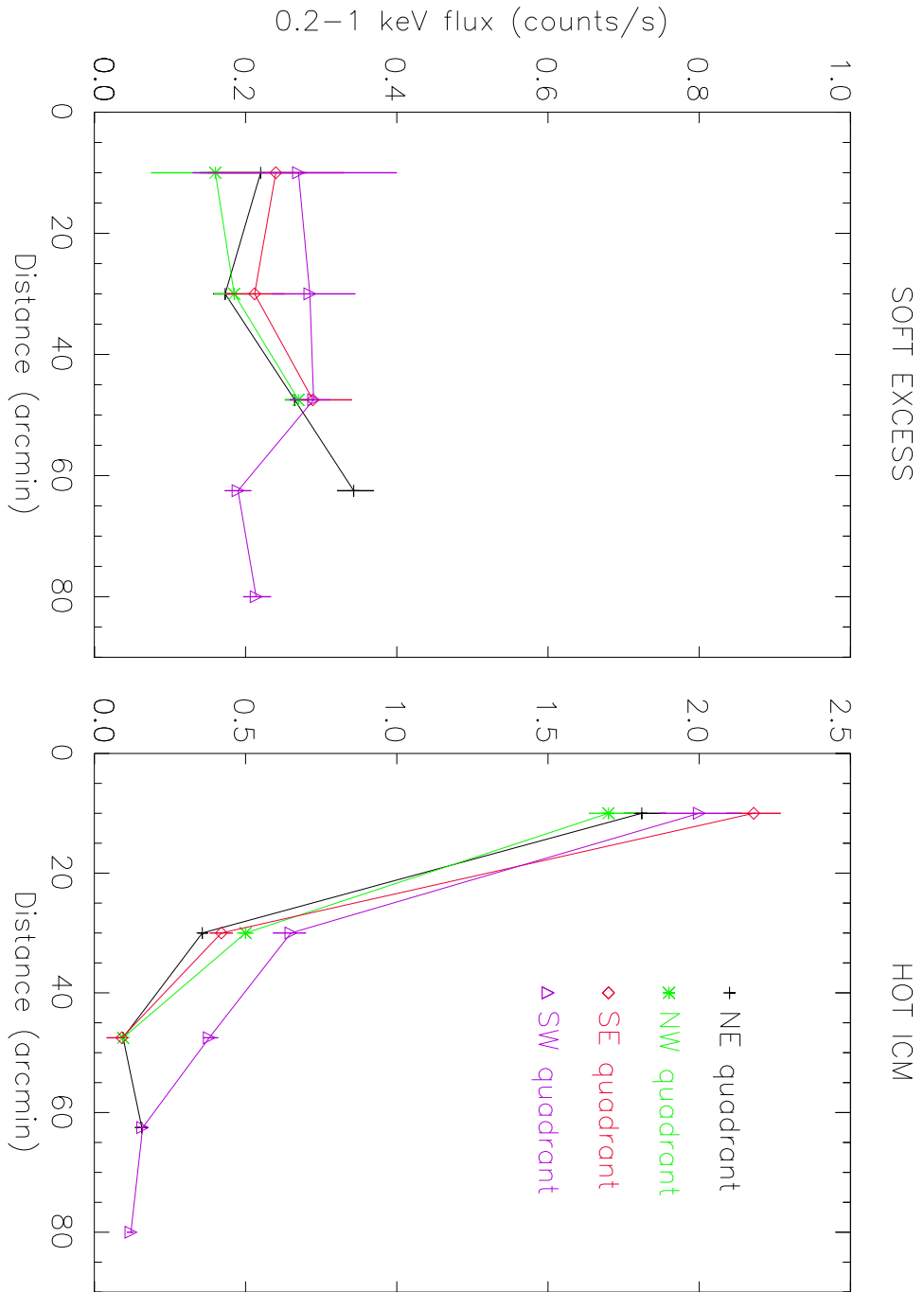


Fig. 5.— The radial distribution of the soft excess emission and of emission from the hot ICM



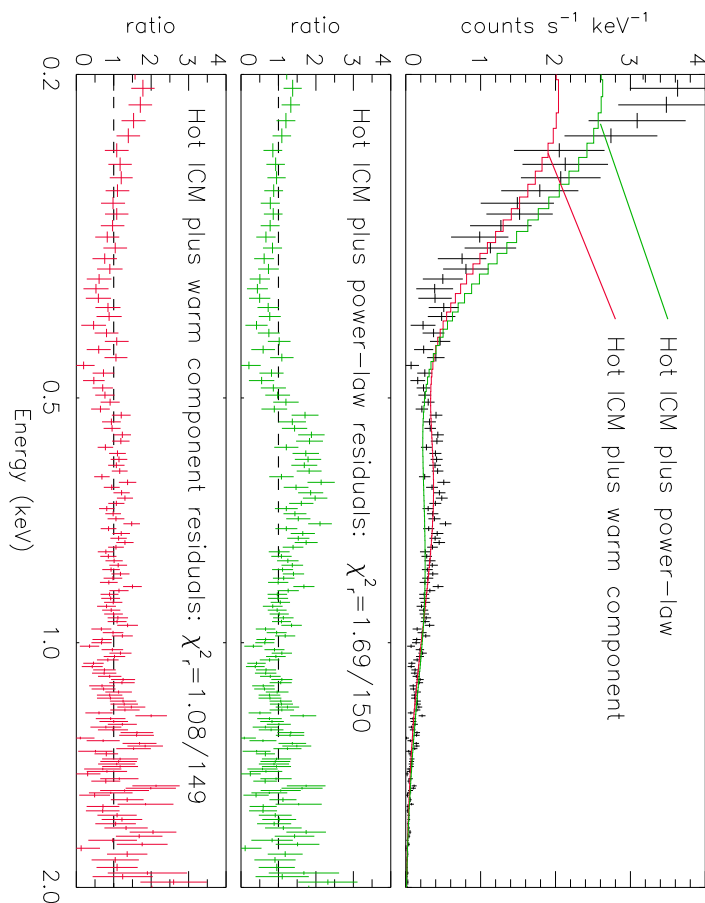


Fig. 6.— *ROSAT* PSPC spectrum of the 50-70' north-eastern quadrant. In green is the hot ICM plus power law model (section 4.4), in red the hot ICM model plus a low-energy thermal component (section 4.5).

Table 1. Best-fit single temperature models

Region (arcmin)	0.2-2 keV fit, Galactic $N_H$			0.2-2 keV fit, free $N_H$			
	kT (keV)	A	$\chi_r^2/\text{d.o.f}$	$N_H$ ( $10^{19} \text{ cm}^{-2}$ )	kT (keV)	A	$\chi_r^2/\text{d.o.f}$
0-20	$3.9 \pm 0.15$	0.25	9.74/181	$6.15 \pm 0.1$	$6.5 \pm_{0.3}^{0.4}$	0.3	2.8/180
20-40	$2.4 \pm 0.1$	0.2	7.4/181	$2 \pm 0.3$	$3 \pm_{0.1}^{0.3}$	0.2	3.7/180
40-55	$2.3 \pm_{0.1}^{0.1}$	0.2	6.2/175	$\leq 0.01$	$2.3 \pm 0.1$	0.2	4.2/174
50-70	$1.8 \pm_{0.1}^{0.3}$	0.2	3.5/151	$\leq 0.02$	$1.85 \pm_{0.1}^{0.4}$	0.2	2.9/150
70-90	$1.9 \pm_{0.1}^{0.3}$	0.2	3.1/139	$\leq 0.02$	$2 \pm_{0.3}^{0.5}$	0.2	2.5/138

Table 2. Best-fit hot ICM model and soft X-ray fluxes

Region (arcmin)	Hot ICM			soft X-ray fluxes <sup>(*)</sup>	
	kT (keV)	$I^{(**)}$	$\chi_r^2/\text{dof}$	measured flux (c s <sup>-1</sup> )	hot ICM prediction <sup>(***)</sup> (c s <sup>-1</sup> )
0-20 ALL	7 ±0.25	23.6±0.1	1.42/100	8.85±0.016	8.0 ± <sup>0.05</sup> <sub>0.075</sub> ± <sup>0.22</sup> <sub>0.23</sub>
NE	5.8 ±0.4	4.9±0.1	0.82/100	2.03±0.007	1.81± <sup>0.02</sup> <sub>0.02</sub> ± <sup>0.06</sup> <sub>0.04</sub>
NW	6.6 ±0.6	5.0±0.05	0.89/98	1.86±0.007	1.7± <sup>0.035</sup> <sub>0.025</sub> ± <sup>0.05</sup> <sub>0.04</sub>
SE	6.8 ±0.5	6.6±0.05	0.82/98	2.42±0.008	2.18± <sup>0.03</sup> <sub>0.03</sub> ± <sup>0.06</sup> <sub>0.06</sub>
SW	13.6 ± <sup>2.9</sup> <sub>2</sub>	7.7±0.05	1.01/98	2.27±0.007	2.0± <sup>0.08</sup> <sub>0.08</sub> ± <sup>0.06</sup> <sub>0.05</sub>
20-40 ALL	4.2 ±0.3	6.1±0.05	0.98/100	2.65±0.02	1.88± <sup>0.02</sup> <sub>0.02</sub> ± <sup>0.05</sup> <sub>0.05</sub>
NE	2.6 ±0.3	0.85±0.015	0.69/98	0.53±0.006	0.345± <sup>0.005</sup> <sub>0.005</sub> ± <sup>0.01</sup> <sub>0.01</sub>
NW	4.3 ±0.7	1.65±0.05	0.76/98	0.685±0.007	0.50± <sup>0.011</sup> <sub>0.013</sub> ± <sup>0.015</sup> <sub>0.015</sub>
SE	8 ± <sup>3.2</sup> <sub>2</sub>	1.55±0.03	0.57/98	0.632±0.007	0.42± <sup>0.025</sup> <sub>0.027</sub> ± <sup>0.013</sup> <sub>0.011</sub>
SW	7.8± <sup>2</sup> <sub>1.4</sub>	3.3±0.1	0.89/98	0.935±0.007	0.714± <sup>0.03</sup> <sub>0.04</sub> ± <sup>0.02</sup> <sub>0.02</sub>
40-55 ALL	5.3 ± <sup>2.2</sup> <sub>1.3</sub>	2.9±0.1	0.89/95	1.8±0.038	0.65± <sup>0.03</sup> <sub>0.035</sub> ± <sup>0.015</sup> <sub>0.02</sub>
NE	3.1± <sup>3</sup> <sub>1</sub>	0.33±0.03	0.69/50	0.36±0.01	0.095± <sup>0.005</sup> <sub>0.01</sub> ± <sup>0.003</sup> <sub>0.002</sub>
NW	8.0± <sup>7</sup> <sub>3</sub>	0.42±0.03	0.93/54	0.68±0.015	0.18± <sup>0.013</sup> <sub>0.027</sub> ± <sup>0.005</sup> <sub>0.004</sub>
SE	3.6 ± <sup>8</sup> <sub>1.3</sub>	0.34±0.03	0.96/48	0.38±0.01	0.091± <sup>0.006</sup> <sub>0.026</sub> ± <sup>0.004</sup> <sub>0.025</sub>
SW	3.5 ±0.7	1.6±0.05	1.0/78	0.67±0.01	0.38± <sup>0.015</sup> <sub>0.01</sub> ± <sup>0.015</sup> <sub>0.01</sub>
55-70 ALL	2.6 ± <sup>0.9</sup> <sub>0.5</sub>	0.98±0.05	0.97/136	0.85±0.024	0.3± <sup>0.006</sup> <sub>0.007</sub> ± <sup>0.009</sup> <sub>0.008</sub>
NE	3.5 ± <sup>4.5</sup> <sub>1.3</sub>	0.5±0.04	1.02/70	0.5±0.02	0.137± <sup>0.012</sup> <sub>0.019</sub> ± <sup>0.005</sup> <sub>0.004</sub>
SW	2.3 ± <sup>0.8</sup> <sub>0.5</sub>	0.48±0.04	0.93/65	0.35±0.014	0.16± <sup>0.005</sup> <sub>0.004</sub> ± <sup>0.006</sup> <sub>0.005</sub>
70-90 SW	2.9 ± <sup>2.5</sup> <sub>0.8</sub>	0.42±0.03	1.21/59	0.335±0.014	0.121± <sup>0.005</sup> <sub>0.01</sub> ± <sup>0.005</sup> <sub>0.004</sub>

Note. — (\*) Soft X-ray fluxes are in the 0.2-1 keV band.

(\*\*)  $I$  is the best-fit emission integral in the units of  $(10^{-16}/4\pi((1+z)D)^2)$ , where  $D$  is the distance to the source (in cm) and  $z$  is the redshift.

(\*\*\*) The two error brackets account respectively for the uncertainty in the hot ICM temperature and the uncertainty in the Galactic HI column density ( $\Delta(N_H) = \times 10^{19} \text{ cm}^{-2}$ ).

Table 3. Spectral models

Region (amin)	Non-thermal component		Low energy thermal component				F-test probability (*)
	$\alpha$	$\chi_r^2/\text{d.o.f}$	kT (keV)	A	$I$	$\chi_r^2/\text{d.o.f}$	
0-20 NE	2.65±0.05	1.42/180	0.29±0.05	0.02±0.015	1.3±0.25	1.36/179	61.3%
NW	1.42±0.01	1.54/180	0.25±0.05	0.05±0.03	2.0±1.0	1.18/179	96.2%
SE	1.51±0.02	1.52/180	0.12±0.015	0.07±0.03	1.5±0.5	1.36/179	77.1%
SW	1.40±0.005	1.45/180	0.093±0.01	0.1	0.93±0.06	1.41/180	57.4%
20-40 NE	1.93±0.07	1.45/180	0.22±0.015	0.06± $_{0.02}^{0.05}$	0.7±0.08	1.25/179	83.9%
NW	1.73±0.07	1.59/180	0.21±0.015	0.07± $_{0.03}^{0.06}$	0.8±0.09	1.45/179	73.1%
SE	1.70± $_{0.03}^{0.07}$	1.3/180	0.22±0.015	0.06± $_{0.02}^{0.04}$	0.95±0.06	1.1/179	86.8%
SW	2.30±0.15	1.43/180	0.23±0.08	0.04±0.025	1.45±0.1	1.33/179	68.6%
40-55 NE	2.37±0.05	1.64/131	0.21±0.015	0.1± $_{0.04}^{0.1}$	1.15±0.2	1.1/130	98.8%
NW	2.37± $_{0.04}^{0.07}$	1.15/134	0.21±0.025	0.03± $_{0.02}^{0.035}$	1.7 ±0.15	1.06/133	68.1%
SE	2.44±0.06	1.59/130	0.215±0.015	0.05± $_{0.015}^{0.05}$	1.7 ± 0.2	1.24/129	92.1%
SW	1.91±0.05	1.15/160	0.215±0.025	0.03± $_{0.015}^{0.035}$	2.0±0.2	1.15/159	50.0%
55-70 NE	2.35±0.06	1.69/150	0.20±0.02	0.18± $_{0.08}^{0.17}$	1.2±0.45	1.08/149	99.7%
SW	2.21±0.15	1.40/144	0.23±0.025	0.12± $_{0.05}^{0.07}$	0.7±0.15	1.10 /143	92.5%
70-90 SW	2.2± $_{0.1}^{0.05}$	1.89/140	0.22±0.02	0.15± $_{0.04}^{0.1}$	0.7±0.2	1.41/139	95.8%

Note. — (\*) The F-test describes the likelihood that the thermal model constitutes an improvement over the non-thermal model (Bevington 1969).